Received 15 March 2021; revised 27 April 2021; accepted 31 May 2021. Date of publication 18 June 2021; date of current version 28 June 2021.

Digital Object Identifier 10.1109/OJCOMS.2021.3090399

A Three Dimensional MIMO Channel Model for Unmanned Aerial Vehicle in Urban Environments

HORACIO A. MENDOZA [1,2] AND GRACIELA CORRAL-BRIONES [1]

[1] Laboratorio de Comunicaciones Digitales, Universidad Nacional de Cordoba, Cordoba 5000, Argentina

[2] Grupo de Investigacion y Desarrollo en Ingenieria Electronica, Universidad Nacional de Misiones, Posadas 3304, Argentina

CORRESPONDING AUTHOR: H. A. MENDOZA (e-mail: horacio.mendoza@unc.edu.ar)

This work was supported in part by the National Agency for Science and Technology Promotion of Argentina under Grant PICT-2018-04507; in part by the National Scientific and Technical Research Council of Argentina (CONICET); in part by the Institute for Advanced Studies in Engineering and Technology (IDIT), Argentina; in part by the Universidad Nacional de Cordoba (UNC), Argentina; and in part by the Universidad Nacional de Misiones (UNaM), Argentina.

ABSTRACT Increasing the availability of *Unmanned Aerial Vehicles* (UAV's) platforms leads to a variety of applications for aerial exploration, surveillance, and transport. Many of these applications rely on the communication between the UAV and the ground receiver which is subjected to high mobility that may lead to restrictions on link connectivity and throughput. In order to design high throughput and efficient communication schemes for these scenarios, a deep understanding of the communication channel behavior is required, especially taking into account measurement data from flight experiments. Channel propagation in urban environments involves diffraction effects which modify the *Line-of-Sight* (LoS) contribution of the total received signal, especially when the receiver is located on the ground. This process leads to scenarios where *Multiple-Input Multiple-Output* (MIMO) signal processing can take advantage from this situation. In this context, the goal of this paper is to study the diffraction effects of the LoS component through spatial correlation metrics of the signal. To accomplish this, we propose the use of a geometric stochastic technique to model the channel behavior which lies between *High Altitude Platforms* (HAP) and terrestrial link communications.

INDEX TERMS MIMO, unmanned aerial vehicles, channel model, air-to-ground.

I. INTRODUCTION

DRONES and UAVs are a consolidated technology which support wireless communication systems. Applications like data collection and dissemination for Internet of Things (IoT) nodes at remote sites, as well as data offloading in congested cells in urban areas, represent just a few examples of their utility. However, as the IoT nodes density increases and the cell traffic requires more data offloading, the reliability of the wireless communication needs to be increased [1], [2]. Towards this aim, in the literature body, an important effort on the channel characterization has been summarized in several survey works [3], [4], [5]. In those contributions, the classification of the channels are associated with scenarios, measurement campaigns and analytical channel models available in the literature. Furthermore, there is a consensus that the MIMO communication system is beneficial for increasing the link throughput, however, more measurement campaigns are needed [5].

Nearby scatterers at both link extremes are crucial to exploit MIMO gains. In particular, urban areas offer a propagation structure in which the design of a reliable multiple antenna communication system can be useful. Densely urban areas are characterized by the presence of a large number of buildings, which, in turn, generate long canyons for the propagation signal. This type of environment structure hinders the propagation of some electromagnetic components of the signal. Considering electromagnetic signals contribution consisting of a line-of-sight (LoS) component and Non-line-of-sight components (NLoS), the former results especially attenuated in dense urban environments [6], [7]. The main effect that operates behind this attenuation is the diffraction effect. From the point of view of communication systems that take advantage of multiple antennas to

increase the gain of the received signal, this diffraction effect can be counterproductive. Nevertheless, from the point of view of the multiplexing gain, this situation could be beneficial. Despite this observation, there are few papers which consider this characteristic of the densely urban environment [8], [9], [10], [11], that could be useful for MIMO wireless communication techniques.

Studies that take into account characteristics and relationships between multiple antennas and the surrounding geometrical structure are reported in [3], [4], [5], [12]. According to these contributions, measurement campaigns for Air-to-Ground (A2G) channel characterization have been conducted primarily for Single-Input Single-Output (SISO) link communication systems, especially for channel characterization on airport scenarios and high altitude aircraft flights.

Other multi-antennas A2G channel measurement campaigns have revealed the presence of effects like shadowing due to aircraft maneuvering [13], [14], multipath signal components and a frequent presence of a LoS signal component [6], [12], [15], [16], [17], [18]. A Single-Input Multiple-Output (SIMO) campaign measurement conducted over a near-urban scenario is reported in [19]. Data analysis results show an always-present LoS signal component and multipath component with a delay spread ranging from 10ns to 180ns, suggesting that the effective scatterers are nearby the receiver up to 54 meters. In [20] a 4×2 MIMO-A2G measurement campaign at frequency of 1800 MHz from a helicopter is reported considering a suburban scenario. Data analysis shows a delay spread of the multipath channel between 15ns and 150ns with high dependence on the transmit antenna placement and receive antenna radiation characteristics.

In [21] a SIMO 1×4 downlink measurement shows a similar diversity gain level to that obtained in a Rayleigh fading channel with a 1.5λ of inter-elements separations (at 2 GHz). In [22] MIMO channel measurements have been made at a frequency of 915 MHz with two element transmit antenna array mounted on the aircraft and a configurable linear uniform antenna array at the receiver side (on ground). Data analysis revealed evidence of low spatial channel correlation at both sides of the link and no maneuvering shadowing effects were reported due to the air-frame material. The results of those pieces of research suggest that the LoS signal component cannot be neglected in almost every possible A2G scenario. Therefore, the small scale statistics combined with large scale statistics should be taken into account for every element of the receiver antenna array. Furthermore, the work of [22] clearly indicates that apart from the presence of signal LoS components, the evidence of low spatial channel correlation suggests that some level of multiplexing gain can be exploited to increase the A2G data rate. On the other hand, for maneuvering effects, more MIMO measurements reports are needed to understand how to deal with it.

A good A2G channel model should reflect the latter mentioned channel characteristics in a realistic manner. In general, high altitude SISO-A2G propagations are mainly represented on the basis of a two-ray model [23], [24] or stochastic model [18], [25], [26], [27], [28], [29]. Furthermore, among the accepted MIMO channel modeling options, Geometry-Based Stochastic Channel Model (GBSCM) have gained much attention due to their capability of providing an angular response in a direct way enabling a straightforward computation of spatial and temporal correlation properties [30]. In this sense, a multiantenna extension of the Geometric Air-to-Ground Ellipsoidal (GAGE) radio channel model has been recently proposed by Wentz and Stojanovic [31] for a base station replacement in cellular service. That model considers scatterers uniformly distributed on space and results are based on parallel antenna arrays disposition between Tx and Rx which suggest that different antenna array configuration could not show the same communication link performance. In Blandino *et al.* [32], a wideband multi-antenna extension of (GAGE) radio channel model is proposed for en-route and takeoff/arrival scenarios channel testbed for communication link. That work presupposes a uniform scatterer distribution in a two dimensional space to model the multipath contribution, neglecting the effect of the scatterer's height on the communication link. More recently, Zeng *et al.* [8] proposed a 3D-GSCM A2G channel model considering that the effective scatterers lie within a cylindrical volume around the receiver. However, the proposed model does not consider the LoS signal component on the results.

All the aforementioned pieces of research consider single-bounced multipaths contributions of scatterers distributed within an elliptical or cylindrical volume space. For low altitude UAV-A2G channels in urban scenarios, the main multi-path contribution comes from nearby scatterers and it requires many geometric parameters to generate signal models. In this sense, a cylindrical scatterer geometry has the advantage of requiring less parameters and computational effort than an elliptical configuration and could be more appropriate to characterize the A2G channel. In a previous work [33], we showed the potential benefits of the aforementioned model applied to the A2G scenario. Since the LoS signal component cannot be neglected in emerging low-altitude UAV-A2G scenarios and the buildings take a special relevance on urban environments, it is clear that the geometry of the scenarios is somewhere between HAP communication and terrestrial link. In this paper, we propose a new A2G three dimensional reference model that takes into account the diffraction of LoS component and single-bounced multipaths contribution of the cylindrical scatter geometry. In the same work, more information has been provided regarding the potential benefits for applying a HAP-MIMO channel model to a scenario where one end is a UAV and the other end is immersed in an urban environment. In addition, low altitude urban scenario key limitations were identified since the original model was intended for High Altitude Platforms.

Identifying the assumptions and contrasting them with new UAV scenarios in dense urban environments is an extremely

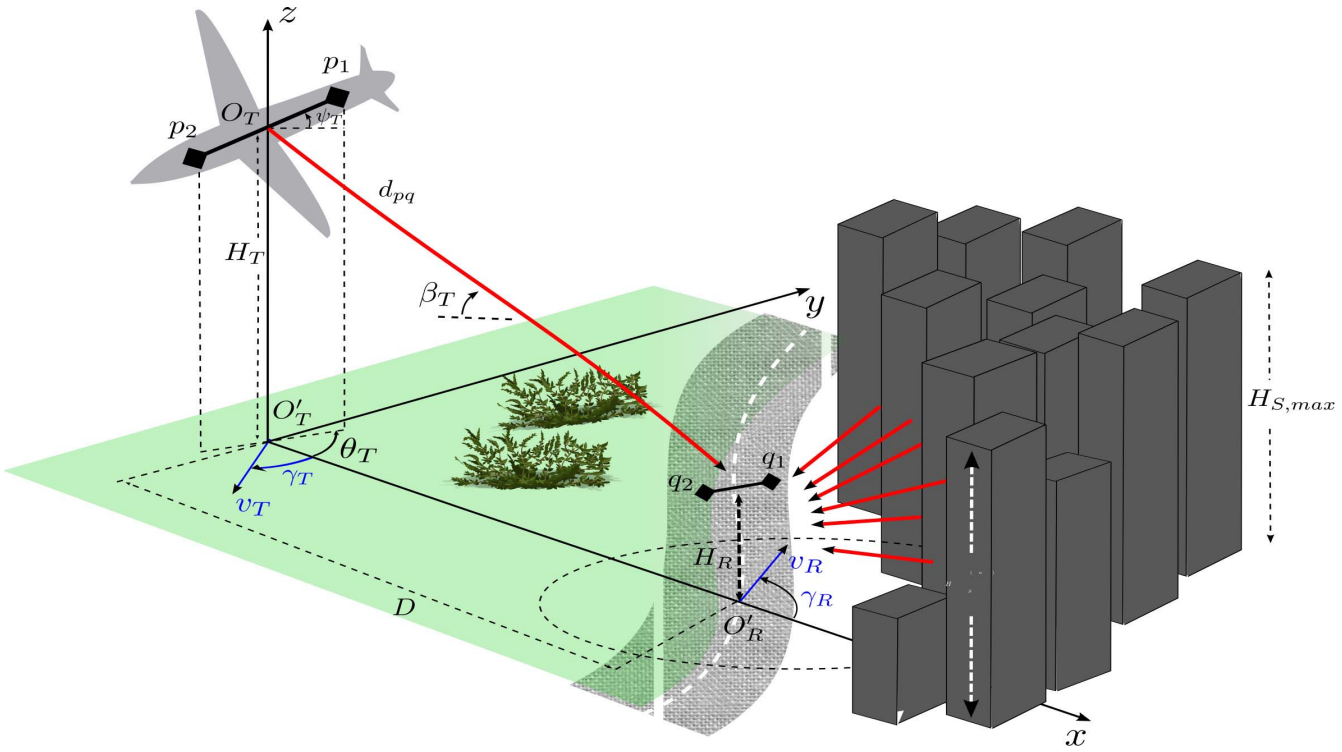

FIGURE 1. Geometrical 3D MIMO channel Model. LoS diffracted path component.

necessary exercise, since computing the link path neglecting the distance between the antenna elements [8] is not a realistic consideration in these cases. That is the reason why in this work the original HAP model is extended enabling its use in new scenarios, especially in dense urban scenarios, resulting in a new channel model. Furthermore, the proposed model can be used for channel simulation, having defined the channel coefficients, they can be used to study the channel behavior. Also, the space-time correlation analysis exposes the advantages of the three dimensional model through the statistical similarities of the channels configured between the interelements of the antenna arrays. Finally, the proposed model can be validated with AG channel measurement campaigns performed at low height in urban scenarios. This can be performed by using small and medium UAV with restricted payload capacity requiring portable channel-sounder equipment of low weight and size.

The main contributions of this work are:

1) The identification that the diffraction effect is beneficial for MIMO communication in densely urban settings.
2) The development of a new stochastic geometric model, based on the extension of the Michailidis model which allows it to operate in densely urban environments where link distances are shorter than the original model.

This work is organized as follows. In Section II, 3D-UAV MIMO channel model is described. In Section III the corresponding space-time correlation function is derived. Section IV shows numerical results of transmit and receive correlation. Section V discusses the conclusion of this work.

II. THREE-DIMENSIONAL GBSM FOR UAV-MIMO CHANNELS

In this section we describe a new channel model for urban UAV-MIMO scenarios. In downlink condition, the signal travels from the UAV-transmitter to the ground-receiver through the buildings that surrounds the receiver. The presence of several buildings and the relative low altitude of UAV flight, configure an scenarios where the receiver signal exhibits intermittent diffracted direct path and reflected components, which is why a 3D model is required in order to describe them.

A. GEOMETRIC MODEL PARAMETERS

This model considers outdoor radio propagation where the direct path (LoS) is affected by diffractions effects and single-bounced reflections path (NLoS) are present en each channel. The set of channels, at time t, are described by a $L_R \times L_T$ MIMO matrix, H(t), with $L_R \times L_T$ time variant complex low-pass impulses responses.

The geometrical characteristic of the scenario is shown in Fig. 1 and Fig. 2, for LoS and NLoS component respectively. Note that in Fig. 2 a diffracted LoS component is remarked. The parameter definition over a Cartesian coordinates are listed in Table 1.

In this $L_R \times L_T$ MIMO configuration, Uniform Linear Antenna arrays (ULA) are used. The spacing between two

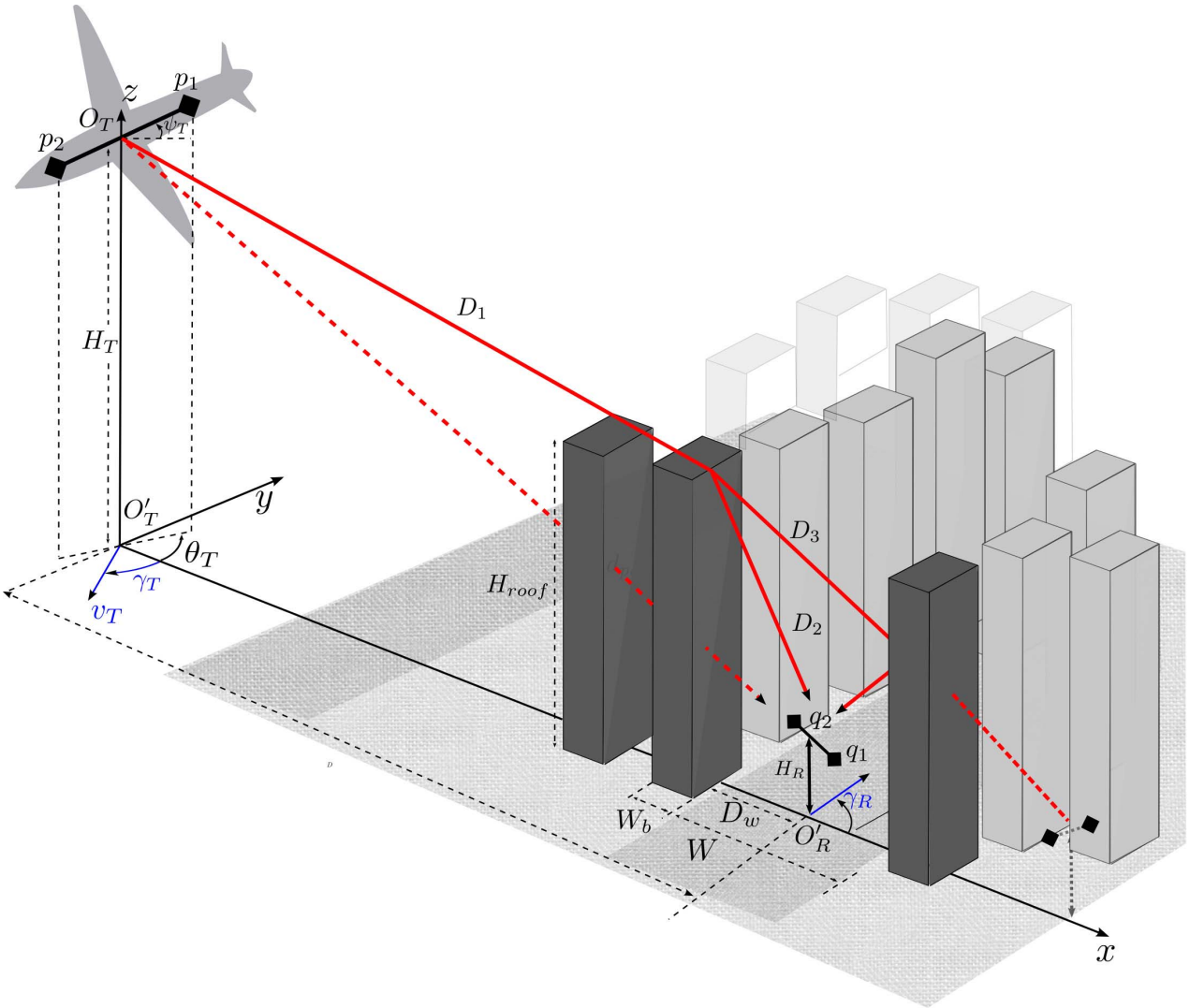

FIGURE 2. Geometrical 3D MIMO channel Model. NLoS path component.

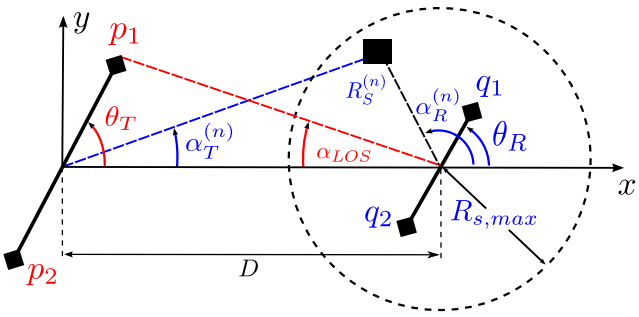

FIGURE 3. Angles definition on $x-y$ plane.

adjacent antenna elements, at both transmitter (Tx) and receiver (Rx) array, is denoted by δ_T and δ_R, respectively. Transmitter and receiver antenna array's heights are denoted by H_T and H_R, respectively; The distance of two points is denoted by $d(a, b)$; the distance between points a and b. θ_T and θ_R are the angles that describe the orientation of the Tx and Rx antenna array on the $x-y$ plane, respectively (see Fig. 3), and angle ψ_R describes the elevation of the Rx's antenna array relative to the $x-y$ plane.

Considering that the geometry of this scenarios is somewhere between HAP communication scenario and terrestrial link scenario, it's assumed that the elevated transmitter array is still free of scatterers and the receiver array is located on the ground and surrounded by scatterers. The scatterers around the receiver lie inside of a cylinder of radius $R_{S,max}$ and height of $H_{S,\max}$. The n^{th} scatterer is located by $R^{(n)}$, and $H^{(n)}$ that represents the radius and the height of the scatterer relative to O'_R, respectively. The elevation angle of the Tx relative to the Rx is given by

$$\beta_T = \arctan\left(\frac{H_T - H_R}{D}\right), \tag{1}$$

and considering that, $H_{S,max} >> H_R$, the elevation angle of the n^{th} scatterer relative to the centre of the receiver array

TABLE 1. Geometrically model parameters definitions.

L_T, L_R	Elements number of Tx and Rx array, respectively.
D	Distance (in $x-y$ plane) between the centres of Tx and Rx array.
$R_{s,max}$, $H_{s,max}$	Radius and height of the cylinder with the scatterers, respectively.
δ_T, δ_R	The spacing between antenna array elements.
θ_T, θ_R	Orientation of the UAV and *Ground Station* (GS) antenna array in the $x-y$ plane (relatively to x axis) respectively.
ψ_T, ψ_R	Elevation angle of the p^{th} and q^{th} antenna element, respectively.
v_T, v_R	Speed of the UAV and GS respectively.
γ_T, γ_R	The moving direction (in $x-y$ plane) of the UAV and GS, respectively.
$f_{T,max}$, $f_{R,max}$	The maximum Doppler frequency shift of the UAV and GS, respectively.
β_T	Elevation angle of the UAV relative to the centre of the array of GS.
H_T, H_R, $H_S^{(n)}$	The height of the UAV, the GS and the n^{th} scatterer, respectively.
α_{LoS}	The azimuth angle of arrival of the LoS path.
$\varphi^{(n)}$, $g^{(n)}$	The random phase and the amplitude introduced by the n^{th} scatterer, respectively.
$\alpha_R^{(n)}$, $\alpha_T^{(n)}$	The azimuth angle of arrival an the azimuth angle of departure at/from the n^{th} scatterer, respectively.
$R_s^{(n)}$	The distance between the centre of the RX array and the n^{th} scatterer in the $x-y$ plane.
$\beta_S^{(n)}$	The elevation angle of the n^{th} scatterer relative to the centre of the RX array.
Ω_{pq}	Power associated with the pq^{th} planar wave.
D_1	Distance from Tx to the rooftop of the last building.
D_2	Distance from the last building rooftop to the Rx.
D_3	Distance from the last building rooftop to the Rx, through rear building reflection.
H_{roof}	Last building height.
D_w	Distance from the last building to the Rx, in $x-y$ plane.
W	Street width.
W_b	Last building width.
K_{pq}	Rician factor of the pq channel.
ν	Normalized obstruction.

(O_R) can be approximated by

$$\beta_S^{(n)} = \arctan\left(\frac{H_S^{(n)} - H_R}{R_S^{(n)}}\right). \tag{2}$$

It's assumed that Tx and Rx are moving with speeds v_T and v_R in directions described by azimuthal angles γ_T and γ_R, respectively. Since is considered the aircraft flights in a circle with constant altitude, v_T is related to the angular velocity of the transmitter as

$$v_T = \zeta RT, \tag{3}$$

where ζ is the angular frequency, T is the time period, and R is the radius of the rotation of the aircraft. As a consequence, γ_T is always perpendicular to circular flight radius (R_T).

B. SIGNAL MODEL PARAMETERS

UAV link channels are expected to behaves as Rician in its general form. For the channel between the p^{th} transmit and q^{th} receive antenna, the channel impulse response (CIR), under frequency-flat fading consideration, can therefore be written as a superposition of LoS and NLoS rays, i.e.,

$$h_{pq}(t) = h_{pq,LoS}(t) + h_{pq,NLoS}(t), \tag{4}$$

Note that we consider here that the LoS component already affected by the diffraction effects. Since the number of local scatterers is considered infinite, the central limit theorem implies that $h_{pq}(t)$ is a low-pass nonzero-mean complex Gaussian process. Hence, the envelope $|h_{pq}(t)|$ is a Rice process. In addition, $h_{pq,NLoS}(t)$ is a low-pass zero-mean complex Gaussian process, and the envelope $|h_{pq,NLoS}|$ is Rayleigh distributed, while $h_{pq,LoS}(t)$ is a deterministic process.

Each term of the CIR in (4) can be written as,

$$h_{pq,LoS}(t) = \sqrt{\frac{K_{pq}\Omega_{pq}}{K_{pq}+1}} \exp\left(-j\frac{2\pi}{\lambda}d(p,q)\right) \times \exp\left(j2\pi t\left[f_{T,LoS} + f_{R,LoS}\right]\right), \tag{5}$$

$$h_{pq,NLoS}(t) = \sqrt{\frac{\Omega_{pq}}{K_{pq}+1}} \lim_{N\to\infty} \frac{1}{\sqrt{N}} \sum_{n=1}^{N} g^{(n)} \times \exp\left(-j\frac{2\pi}{\lambda}\left[d\left(p, S^{(n)}\right) + d\left(S^{(n)}, q\right)\right]\right) \times \exp\left(j\varphi^{(n)}\right) \times \exp\left(j2\pi t\left[f_{T,NLoS} + f_{R,NLoS}\right]\right), \tag{6}$$

where $f_{T,LoS}$, $f_{R,LoS}$, $f_{T,NLoS}$, and $f_{R,NLoS}$ are Doppler shifts component. Ω_{pq} and K_{pq} are the power and the Rician factor of the pq channel respectively. All of these explained with more details in the next sections.

1) DIFFRACTION

Diffraction effects take place when an obstructing edge are present on the direct path of the signal. UAV links configure a different geometric scenario for the diffraction attenuation calculation than terrestrial link. In this case the receiver is located much closer to the obstruction, so their effects cannot be model as the single knife obstruction located in the center of the Tx-Rx path. To model this effect we adopt a similar approach as the work of Simunek *et al.* [7] where the excess loss attenuation due to diffraction is modeled by broken down the direct path in two parts, each being affected by different diffraction mechanism, see Fig. 2. The first part, the line of sight between the transmitter and the top of the last building before the receiver, is affected by diffraction effects known as secondary knife-edge attenuation. For the second part of the direct ray we need to look closer to the received signal

at the street level. The received signal at street level may be composed of many rays, the most significant considered in this work are the direct and the specular rays. The former reaches at the receiver after being diffracted on the building closer to the transmitter side, and the latter is reflected ray on the building at the opposite side of the street, which undergo diffraction effects before being reflected. To keep the model simple we consider the effects of the diffraction from the last building only. This diffracted attenuation is a results of combinations of three factors, this is

$$h_{D,pq} = \left(h_{lb,D} + R_b h_{lb,R}\right) h_{lb,2}, \tag{7}$$

where $h_{lb,D}$ and $h_{lb,R}$ are the attenuation of direct ray and reflected ray of the main diffracting edge. R_b is the reflection coefficient and $h_{lb,2}$ is the attenuation of secondary knife-edge where the subindex *lb* refers to *last building*. To compute the excess loss based on each attenuation factor, we use the following approximations,

$$|h| = \begin{cases} 1 - e^{-0.60380.1094^{\nu}}, & \text{for } \nu < 0, \\ 0.5e^{-0.95\nu}, & \text{for } 0 \geq \nu \leq 1, \\ \frac{0.225}{\nu}, & \text{for } \nu > 1, \end{cases} \tag{8}$$

then in equation (7) we obtain the total attenuation by diffraction, where $|h_{D,pq}| = \frac{|h_{pq}|}{|h'_{pq,LoS}|}$ the ratio of the actual received field and the free space under line of sight conditions and ν is the normalized obstruction parameters, see Fig. 4. For the calculation of ν we use the available geometry of the scenario, e.g., for the direct ray of the main diffracting edge of Fig. 2

$$D_1 = \sqrt{(D - D_w)^2 + \left(H_T - H_{roof}\right)^2}, \tag{9}$$

$$D_2 = \sqrt{D_w^2 + \left(H_{roof} - H_R\right)^2}, \tag{10}$$

$$\Delta_1 = D_1 + D_2 - d(O_T, O_R), \tag{11}$$

then,

$$\nu = \sqrt{4|\Delta_1|/\lambda}; \tag{12}$$

for the reflected ray, similar calculation can be performed then, the direct ray and reflected ray are added coherently. Then the actual LoS field strength is given by

$$h_{pq,LoS} = \left(h_{D,pq}\right)\left(h'_{pq,LoS}\right), \tag{13}$$

where $h'_{pq,LoS}$ is the free space loss attenuation.

2) CHANNEL GAINS

The transmitted power of the channel pq is assumed to be unitary, i.e., $\Omega_{pq} = E\{|h_{pq}(t)|^2\} = 1$, where $E\{\cdot\}$ is the statistical expectation operator. The power of the NLoS component, $E\{|h_{pq,NLoS}(t)|^2\}$, is assumed to be $1/(K_{qp}+1)$, therefore from (6),

$$\frac{1}{N}\sum_{n=1}^{N} E\left\{\left|g^{(n)}\right|^2\right\} = 1, \quad \text{as } N \to \infty. \tag{14}$$

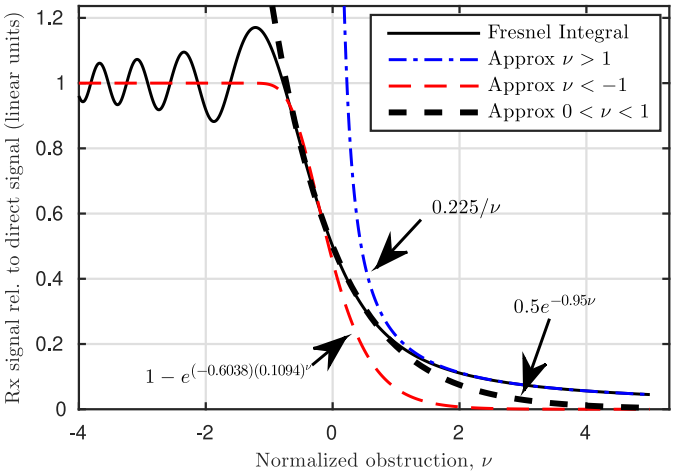

FIGURE 4. Fresnel integral approximation used to calculate the excess loss of each diffracted path involved in the total LoS attenuation at the receiver side.

Then

$$K_{pq} = \frac{\left|h_{pq,LoS}(t)\right|^2}{\left|h_{pq,NLoS}(t)\right|^2}, \tag{15}$$

describes how the total signal power, between the p^{th} transmit and the q^{th} receive element of the antenna array, is split between the LoS and NLoS components. Note that due to the intermittent presence of building, the main effects that LoS component undergo is an attenuation relative to LoS component without obstructions, resulting in a variable Rice factor K as equation (13) predicted. In addition to this, if $\max(\delta_T, \delta_R) << D$, the Rician fading factor could be assumed to be the same for all antenna elements.

3) PHASES

It's assumed that the phase $\varphi^{(n)}$ is a random variable uniformly distributed on the interval $[-\pi, \pi)$, and independent of from $\alpha_T^{(n)}$, $\alpha_R^{(n)}$, $R_S^{(n)}$, $H_S^{(n)}$ and $\beta_S^{(n)}$.

4) PATH LENGTHS

In this new scenario Tx-Rx path length does not hold the assumption that $R_{S,\max} << D$, so the distances $d(p,q)$, $d(p,S^{(n)})$, and $d(S^{(n)},q)$ are calculated as follows:

$$d(p,q) = \Big[\left(D + D_{R_x} - D_{T_x}\right)^2 + \left(D_{R_y} - D_{T_y}\right)^2 + \left(H_T + D_{T_z} - H_R - D_{R_z}\right)^2\Big]^{1/2}, \tag{16}$$

$$d\left(p, S^{(n)}\right) \approx \Bigg[\left(R_S^{(n)}\right)^2 + D^2 - 2R_S^{(n)} D\cos(\pi - \alpha_T) + \left(\frac{\delta_T}{2}(L_T + 1 - 2p)\right)^2 + - \frac{D\sin\alpha_R^{(n)}}{\sin\left(\alpha_R^{(n)} - \alpha_T^{(n)}\right)}(L_T + 1 - 2p)\delta_T$$

$$\times \cos\left(\theta_T - \alpha_T^{(n)}\right)\Big]^{1/2} \times \frac{1}{\cos(\beta_T)}, \tag{17}$$

$$d\left(S^{(n)}, q\right) \approx \frac{R_S^{(n)}}{\cos\beta_S^{(n)}} - D_{R_x}\cos\alpha_R^{(n)}\cos\beta_S^{(n)} - D_{R_z}\sin\beta_S^{(n)} - D_{R_y}\sin\alpha_R^{(n)}\cos\beta_S^{(n)}, \tag{18}$$

where

$$D_{T_x} = \frac{1}{2}(L_T + 1 - 2p)\delta_T\cos\theta_T\cos\psi_T, \tag{19}$$

$$D_{T_y} = \frac{1}{2}(L_T + 1 - 2p)\delta_T\sin\theta_T\cos\psi_T, \tag{20}$$

$$D_{T_z} = \frac{1}{2}(L_T + 1 - 2p)\delta_T\sin(\psi_T) \tag{21}$$

$$D_{R_x} = \frac{1}{2}(L_R + 1 - 2q)\delta_R\cos\theta_R\cos\psi_R, \tag{22}$$

$$D_{R_y} = \frac{1}{2}(L_R + 1 - 2q)\delta_R\sin\theta_R\cos\psi_R, \tag{23}$$

$$D_{R_z} = \frac{1}{2}(L_R + 1 - 2q)\delta_R\sin\psi_R, \tag{24}$$

where parameters p and q take values from the sets of array antenna elements $p \in \{1, 2, \ldots, L_T\}$ and $q \in \{1, 2, \ldots, L_R\}$.

5) DOPPLER SHIFTS

Doppler shifts depends on the geometrical relation between the azimuthal directions of movement of Tx and Rx (γ_T and γ_R) and the directions determined by the angles of departure and angles of arrival. Then

$$f_{T,LoS} = f_{T,\max}\cos(\pi - \alpha_{LoS} + \gamma_T), \tag{25}$$

$$f_{R,LoS} = f_{R,\max}\cos(\alpha_{LoS} - \gamma_R), \tag{26}$$

$$f_{T,NLoS} = f_{T,\max}\cos\left(\alpha_T^{(n)} - \gamma_T\right) \tag{27}$$

$$f_{R,NLoS} = f_{R,\max}\cos\left(\alpha_R^{(n)} - \gamma_R\right)\cos\beta_S^{(n)}, \tag{28}$$

where $f_{T,\max} = v_T/\lambda$ and $f_{R,\max} = v_R/\lambda$, are the maximum Doppler frequencies associated with the UAV and the ground station, respectively and λ is the carrier wavelength. α_{LoS} and $\alpha_T^{(n)}$ are given by

$$\alpha_{LoS} = \pi - \tan\left[\frac{D_{T_y}}{(D - D_{T_x})}\right]^{-1}, \tag{29}$$

$$\alpha_T^{(n)} = \tan\left[\frac{R_S^{(n)}\sin\alpha_R^{(n)}}{D + R_S^{(n)}\cos\alpha_R^{(n)}}\right]^{-1}. \tag{30}$$

III. SPATIAL-TEMPORAL FADING CHARACTERISTICS

The space-time correlation function between two arbitrary channels h_{pq} and h_{lm} is defined as

$$R_{pq,lm}(\delta_T, \delta_R, \tau, t) = \frac{E\{h_{pq}(t)h_{lm}(t+\tau)^*\}}{\sqrt{\Omega_{pq}\Omega_{lm}}}, \tag{31}$$

taking into consideration that the NLOS component of both channels are zero mean process, the space-time correlation function can be written as

$$R_{pq,lm}(\delta_T, \delta_R, \tau, t) = R_{pq,lm}^{LoS}(\delta_T, \delta_R, \tau, t) + R_{pq,lm}^{NLoS}(\delta_T, \delta_R, \tau, t), \tag{32}$$

where $R_{pq,lm}^{LoS}(\delta_T, \delta_R, \tau, t)$ and $R_{pq,lm}^{NLoS}(\delta_T, \delta_R, \tau, t)$ denotes the space-time correlation function of the LoS and NLoS component, respectively. As in [34] each component can be written as,

$$R_{pq,lm}^{LOS}(\delta_T, \delta_R, \tau) = \sqrt{\frac{K_{pq}K_{lm}}{(K_{pq}+1)(K_{lm}+1)}} \times \exp\left(d(p,q) - d(l,m)\right) \times \exp\left(-j2\pi\tau f_{T,\max}\cos(\pi - \alpha_{LoS} + \gamma_T)\right) \times \exp\left(-j2\pi\tau f_{R,\max}\cos(\alpha_{LoS} - \gamma_R)\right), \tag{33}$$

$$R_{pq,lm}^{NLoS}(\delta_T, \delta_R, \tau) = \sqrt{\frac{1}{(K_{pq}+1)(K_{lm}+1)}} \times \int_0^{H_{S,\max}}\int_{R_{S,\min}}^{R_{S,\max}}\int_{-\pi}^{\pi} f_{\alpha_R}(\alpha_R)f_{R_S}(R_S)f_{H_S}(H_S) \times \exp\Bigg(-j\frac{2\pi}{\lambda}\big[d(p,S) + d(S,q) - d(l,S) - d(S,m)\big]\Bigg) \times \exp\Bigg(-j2\pi\tau f_{T,\max}\cos \times \left(\frac{R_S\sin\gamma_T\sin\alpha_R}{D + R_s\cos\alpha_R} - \gamma_T\right)\Bigg) \times \exp\left(-j2\pi\tau f_{R,\max}\cos(\alpha_R - \gamma_R)\cos\beta_S\right) \times (d\alpha_R)(dR_S)(dH_S), \tag{34}$$

where discrete variables $\alpha_R^{(n)}$, $R_S^{(n)}$, $\beta_S^{(n)}$ and $H_S^{(n)}$, have been replaced by continuous variables (the number of scatterers are infinity), i.e., α_R, R_S, β_S, and H_S with joint probability density function (pdf),

$$f(\alpha_R, R_S, H_S) = f_{\alpha_R}(\alpha_R)f_{R_S}(R_S)f_{H_S}(H_S). \tag{35}$$

Several distribution can be used to characterize the azimuth angle α_R (Uniform, Laplacian, Von Mises, etc). Due to the increasingly interest in urban and suburban scenario we use the well justified Von Mises pdf [35]. The Von Mises pdf is defined as

$$f_{\alpha_R}(\alpha_R) = \frac{\exp(\kappa\cos(\alpha_R - \mu))}{2\pi I_0(\kappa)}, \quad -\pi \le \alpha_R \le \pi \tag{36}$$

where $I_0(\cdot)$ i the zeroth-order modified Bessel function of the first kind, $\mu \in [-\pi, \pi]$ is the mean angle at which the scatterers are distributed in the $x-y$ plane, and $\kappa \ge 0$ controls the spread around the mean. To characterize the distance R_S, we use the hyperbolic pdf, which is empirically justified in [36]. The hyperbolic pdf is defined as

$$f_{R_S}(R_S) = \frac{a/\cosh^2(aR_S)}{\tanh\left(aR_{S,\max}\right) - \tanh\left(aR_{S,\min}\right)}, \tag{37}$$

where $R_{S,\min} \leq R_S \leq R_{S,\max}$, and $0 \leq a \leq 1$ controls the spread (standard deviation) of the scatterers around the ground station.

Scatterer height H_S, was reported to follow a lognormal [37], normal [38], [39], or Rayleigh distribution [40], depending of the scenario environment. In this work, we adopt the lognormal pdf, which is defined as

$$f_{H_S}(H_S) = \frac{\exp\left(-\frac{[\ln H_S - \ln H_{S,mean}]^2}{2\sigma^2}\right)}{H_S\sigma\sqrt{2\pi}}, \tag{38}$$

with $0 < H_S \leq H_{S,\max}$ and where the parameters $H_{S,mean}$ and σ are the mean and standard deviation of H_S respectively. As a reference, Table 2 shows the stochastic parameters associated with each distribution. The model takes into account urban scenarios and, in this sense, similar parameters were chosen as Vasques-Castro work [37] where the reference scenario is a densely built-up district (London U.K.) in such scenario were found that the building heights follows a lognormal distribution with parameters $H_{S,mean} = 17.6$ m and $\sigma = 0.31$. For the hyperbolic and Von Mises distributions, the parameters were chosen as Michailidis work which was based on a ray tracing technique to set the values considering a typical European urban environment. In the case of measurement data available, the model calibration can be performed using a two stage methodology. In the first stage the multipath parameters can be obtained from the data set and, in the second stage the parameters of the model can be extracted. It is worth mentioning that recent works show that applying machine learning methods have the potential to simplify the process of the first stage [41], [42]. Taking into account the adopted distribution, the space-time correlation function of the NLoS component becomes as is shown in equation (39), shown at the bottom of the page. Finally, the space-time correlation function between two arbitrary channels, h_{pq} and h_{lm}, becomes a summation of the space-time correlation function of the LoS and the NLoS component, defined in (33) and (39), respectively.

TABLE 2. Scatterers distribution parameters.

μ	The mean azimuth angle at which the scatterers, are distributed in the $x-y$ plane (**Von Mises pdf** [37])
κ	The spread of the scatterers around the mean azimuth angle (**Von Mises pdf** [37]).
a	The spread of the scatterers around the GS (**hyperbolic pdf** [38]).
$R_{S,\max}$	The maximum considered Radius (x-y plane distance) (**hyperbolic pdf** [38]).
$R_{S,\min}$	The minimum Radius (x-y plane distance) (**hyperbolic pdf** [38]).
σ	The standard deviation of scatterer's height (**log-normal pdf** [39]).
$H_{S,\text{mean}}$	The mean of the scatterer's height (**log-normal pdf** [39]).
$H_{S,\max}$	The maximum considered height of the scatterer (**log-normal pdf** [39]).

IV. NUMERICAL RESULTS

In this section, we present the transmit and receive correlations and capacity results obtained from numerical simulation. Channel gains, channel correlations and capacities are studied by simulations. In each point of the flight, the signal gathered is considered wide-sense stationary and the changes in polarization matching and antenna pattern are considered insignificant.

A. DIFFRACTION EFFECTS

Figures 5, 6 and 7 show diffraction effects $|h_{D,pq}|^2$ (see eq. (7)) on a static scenario configured as the one used in the work of Simunek *et al.* [7], where the last building, the one closest to the receiver, has a width of $W_b = 17$ m and height of 22 m. The width of the street (W) is assumed 17 m and the Rx is located at $D_w = 15$ m from the main diffracting-edge (see Fig. 2). With those parameters, the LOS diffraction attenuation is estimated with equations (5) to (12) of [7].

$$\begin{aligned} R^{NLoS}_{pq,lm}(\delta_T, \delta_R, \tau) = \frac{1}{K+1} \int_0^{H_{S,\max}} \int_{R_{S,\min}}^{R_{S,\max}} \int_{-\pi}^{\pi} & f_{\alpha_R}(\alpha_R) f_{R_S}(R_S) f_{H_S}(H_S) \\ \times \exp\Bigg(-j\frac{2\pi}{\lambda\cos\beta_T} & \left[\xi + \left(\frac{1}{2}\delta_T(L_t + 1 - 2p) \right)^2 - \sqrt{\xi}(L_t + 1 - 2p)\delta_T \cos(\theta_T - \alpha_T) \right]^{1/2} \Bigg) \\ \times \exp\Bigg(j\frac{2\pi}{\lambda\cos\beta_T} & \left[\xi + \left(\frac{1}{2}\delta_T(L_t + 1 - 2l) \right)^2 - \sqrt{\xi}(L_t + 1 - 2l)\delta_T \cos(\theta_T - \alpha_T) \right]^{1/2} \Bigg) \\ \times \exp\Bigg(j\frac{2\pi}{\lambda}(m-q)\delta_R & \left[cos\theta_R \cos\psi_R \cos\alpha_R \cos\beta_s + \sin\psi_R \sin\beta_s + \sin\theta_R \cos\psi_R \sin\alpha_R \cos\beta_s \right] \Bigg) \\ \times \exp\Big(-j2\pi\tau & \left[f_{T,\max}\cos(\alpha_T - \gamma_T) + f_{R,\max}\cos(\alpha_R - \gamma_R)\cos\beta_s \right] \Big) (d\alpha_R)(dR_S)(dH_S), \end{aligned} \tag{39}$$

with $\xi = R_S^2 + D^2 - 2R_S D\cos(\pi - \alpha_R)$

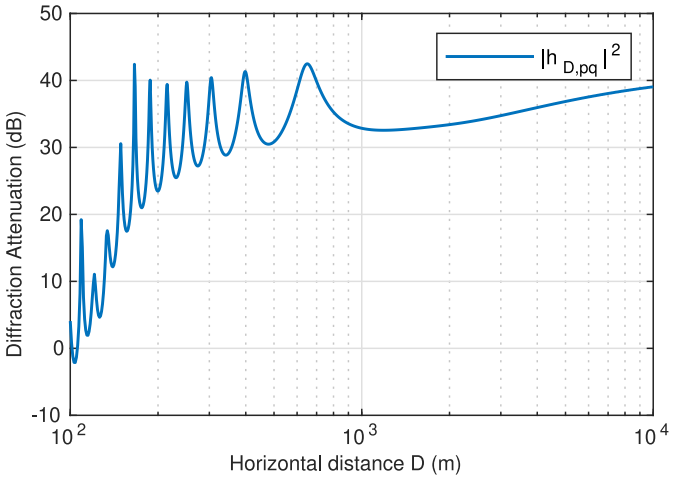

FIGURE 5. Last building attenuation, $|h_{D,pq}|^2$ as a function of the horizontal distance (D), with the UAV transmitting and flying at constant height of $H_T = 150$ m. Geometric scenario parameters set in similar way as [7].

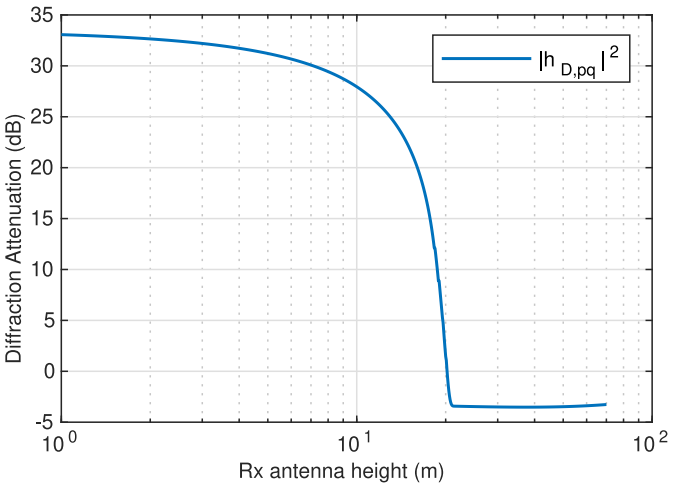

FIGURE 6. Last building attenuation, $|h_{D,pq}|^2$ as a function of the Rx antenna height, H_R. Assuming a fixed horizontal distance of $D = 1000$ m, UAV flying a constant height of $H_T = 150$m and similar geometric scenario configuration as [7].

Fig. 5 shows the effect of the horizontal distance over the last building factor $|h_{D,pq}|^2$ (eq. (7)). The effect of the diffraction can be clear appreciated, with the UAV as a transmitter and flying at constant height of $H_T = 150$ m and similar geometric scenario configuration as [7]. The result shows a LoS component starting to be obstructed from approximately $D \approx 160$ m, suggesting that the main contribution of the diffraction occurs near the receiver and then becomes almost invariant with the horizontal distance D.

Fig. 6 shows the Last building attenuation, $|h_{D,pq}|^2$ as a function of the Rx antenna height, H_R. Result shows a consistent behavior of the diffraction attenuation with the increase of the Rx antenna height. Assuming a fixed horizontal distance of $D = 100$m and the height of the building set a 22m, when the Rx antenna matches this building height the signal strength starts to increase up to reach the LoS signal level. Note the attenuation factor is over 40dB for RX antenna height below to 10m.

Fig. 7 shows the diffraction effect as a function of the height of the UAV ($D = 1000$m, constant), where the level of signal field increases with height until the aircraft is unblocked by the buildings. Note the oscillation of the response, due the constructive and destructive contribution of the different diffracted components. Furthermore, the result indicates that the UAV must achieve an elevation around 1000 m to get a geometric LoS connection with the RX. This result suggests that an UAV flying at low altitude configures a scenario with a highly attenuated LoS component contribution to the received signal. These results are consistent with those shown by Simunek *et al.* [7] in a similar scenario.

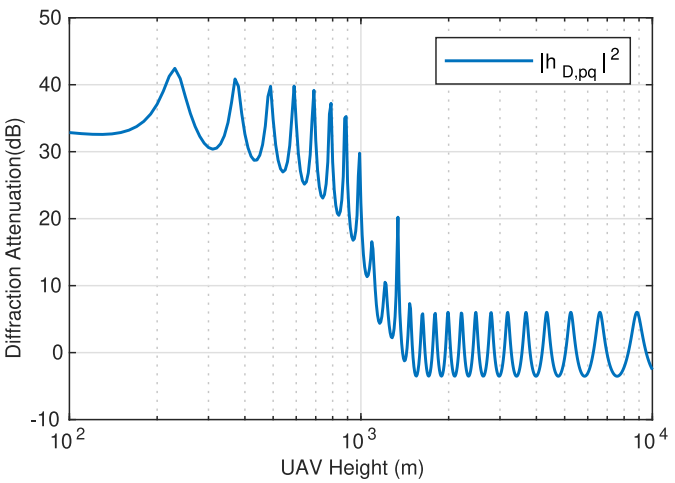

FIGURE 7. Last building attenuation, $|h_{D,pq}|^2$ as a function of the Tx antenna height, H_T. Assuming a fixed horizontal distance of $D = 1000$ m, and similar geometric scenario configuration as [7].

B. SPACE CORRELATION

Unless indicate otherwise, the parameters values used to obtain the curves are listed in Table 3.

Fig. 8 shows the receiver correlation $R_{pq,pm}(\delta_T = 0, \delta_R, \tau, t)$ parametric with the mean height of the surrounded buildings. Results are gathered for two geometric configurations, in the first configuration the transmit and receive array antennas are parallel. In the second case the receive antenna array is vertical, so the three dimensional capability of the model is exhibited. Note that best results correspond to the case of $\psi_R = 0^o$, but with receiver array disposed in almost vertical position ($\psi_R = 60^o$) the correlation results still shows decorrelated behavior beyond 1.5λ of interelement separation.

Fig. 9 shows the transmit correlation $R_{pq,lq}(\delta_T, \delta_R = 0, \tau, t)$ parametric with the elevation angle. The results shows that a correlation levels below that 0.15 could be achieved from a separation of $20\delta_T/\lambda$ on. This results contrast with

TABLE 3. Scenario parameters.

$L_T = L_R = 2$	Elements number of Tx and Rx array, respectively.
$\delta_T = \delta_R = 0^o$	The spacing between antenna array elements.
$\beta_T = 17^o$	Elevation angle of the UAV relative to the centre of the array of GS.
$\theta_T = \theta_R = \pi/2$	Orientation of the UAV and GS antenna array in the $x-y$ plane (relatively to x axis) respectively.
$\psi_T = \psi_R = 0^o$	Elevation angle of the p^{th} and q^{th} antenna element, respectively.
$\gamma_T = \pi/11$	The moving direction (in $x-y$ plane) of the UAV.
$\gamma_R = 0.01$	The moving direction (in $x-y$ plane) of the GS.
$f_{T,max} = 8$ Hz	The maximum Doppler frequency shift of the UAV.
$f_{R,max} = 0$ Hz	The maximum Doppler frequency shift of the GS.
$H_T = 300$ m	The height of the UAV.
$H_R = 1.5$ m	The height of the GS.
$H_{roof} = 22$ m	Last building height.
$D_w = 15$ m	Distance from the last building to the Rx, in $x-y$ plane.
$W_b = 17$ m	Last building width.
$\mu = \pi$	The mean azimuth angle at which the scatterers, are distributed in the $x-y$ plane (**Von Mises pdf** [36])
$\kappa = 0.5$	The spread of the scatterers around the mean azimuth angle (**Von Mises pdf** [36]).
$a = 0.01$	The spread of the scatterers around the GS (**hyperbolic pdf** [36]).
$R_{S,\max} = 200$m	The maximum considered Radius (x-y plane distance) (**hyperbolic pdf** [36]).
$\sigma = 0.31$	The standard deviation of scatterer's height (**log-normal pdf** [39]).
$H_{S,\text{mean}} = 20$m	The mean of the scatterer's height (**log-normal pdf**).
$H_{S,\max} = 60$ m	The maximum considered height of the scatterer (**log-normal pdf**).

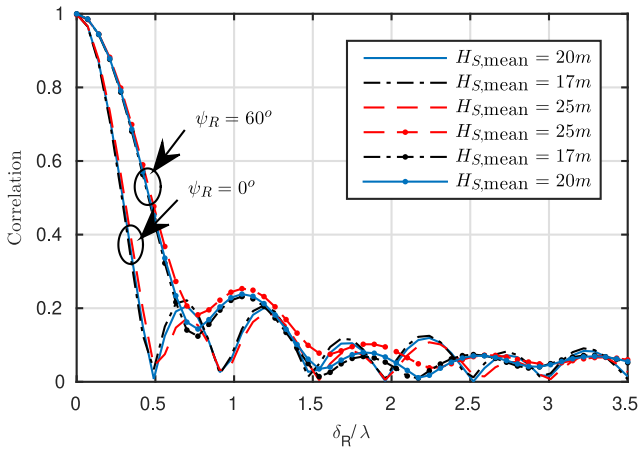

FIGURE 8. Receive Correlation parametric with the average height of the surrounded building ($H_{S,mean}$).

those showed for HAP communication where a longer distance (more than $80\delta_T/lambda$ at similar frequency) are required to achieve the same transmit correlation level.

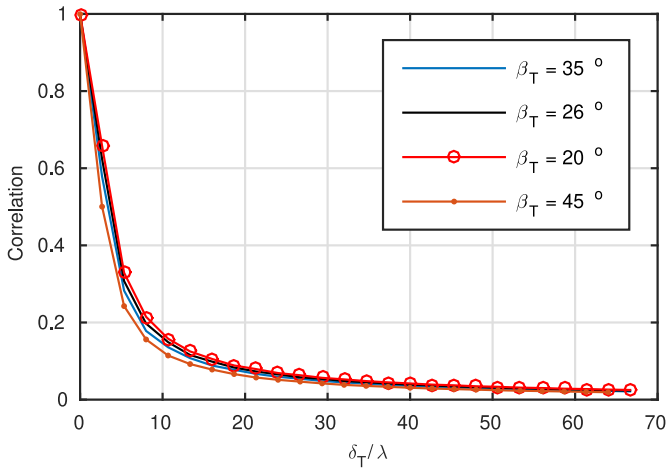

FIGURE 9. Transmit Correlation as a function of interelement spacing and parametric with the elevation angle (β_T).

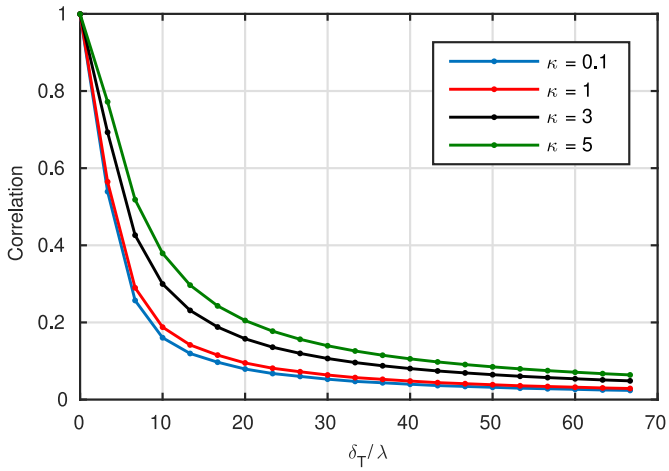

FIGURE 10. Transmit Correlation. Parametric with the spread of the scatterers around the mean azimuth angle (κ).

Fig. 10 shows the transmit correlation parametric with the spread of the scatterers around the mean azimuth angle. It's clear that the best condition for the receiver correlation results from an environment surrounded by scatterers ($\kappa = 0$). On the other hand, if the scatter dispersion decrease, the capacity of the environment to render independent paths (for each receiver antenna) is reduced. This behavior is expected in any environment with consistently non-isotropic scatterer distribution.

V. CONCLUSION

This paper proposes a new three dimensional MIMO channel model for UAV operating in an urban environment. UAV operating at low altitude in urban environments results in a LoS signal component attenuated for more than 30 dB. This type of behavior suggests that the receiver signal component is mainly made of scattered signals. According to the proposed reference scenario, transmit and receive correlation behavior, as a function of inter-element antenna space, were

investigated. Analysis correlation results on the transmitter side show that bringing closer the transmitter increases the signal's interaction with the environment. Thus, it reduces the correlation level. This behavior suggests that it is possible to achieve the same correlation level as HAP channel model counterpart, but this is possible thanks to the small antenna separation. On the other hand, the spread of the scatterer around the receiver plays an important role which renders an independent path for every antenna element, as it is shown in Fig. 10. In that Figure the separation space between the antenna elements of the array is reduced to achieve a minimum 0.15 of correlation level (around $45\delta_T/\lambda$) which is significantly smaller than required by the HAP communication system. Furthermore, the low receive correlation that can be achieved in regions dominated by a non LOS component, can help to mitigate interference. In a SISO channel with LOS component, interference in the ground to air link depends on the height of the UAV. MIMO channels have the potential of exploiting spatial multiplexing to deal with interference. In this model, potential sources of interference are not considered, but the potential of spatial multiplexing is taken into account via space correlation coefficients. From the point of view of the receivers at ground, the small spatial correlation achieved at only 1.5λ inter-element antenna space allows downlink spatial multiplexing to become effective to deal with inter link interference. This is not the case for an uplink spatial multiplexing scheme, since the signals received at UAV are highly correlated. The analyzed channel model assumes the signals in the different links propagate via the same cluster of scatters, which could be not the case when transmitters at ground are far apart. In that case uplink spatial multiplexing may be used to configure multiple uplinks

Our results encourage us to explore further the potential capacity of this type of wireless channel, motivated by the results of correlation levels in both the transmitter and receiver side to find out the benefits of MIMO technology applied to this type of low altitude UAV flight.

REFERENCES

[1] M. Mozaffari, W. Saad, M. Bennis, Y. Nam, and M. Debbah, "A tutorial on UAVs for wireless networks: Applications, challenges, and open problems," *IEEE Commun. Surveys Tuts.*, vol. 21, no. 3, pp. 2334–2360, 3rd Quart., 2019.

[2] N. H. Motlagh, T. Taleb, and O. Arouk, "Low-altitude unmanned aerial vehicles-based Internet of Things services: Comprehensive survey and future perspectives," *IEEE Internet Things J.*, vol. 3, no. 6, pp. 899–922, Dec. 2016.

[3] A. A. Khuwaja, Y. Chen, N. Zhao, M. Alouini, and P. Dobbins, "A survey of channel modeling for UAV communications," *IEEE Commun. Surveys Tuts.*, vol. 20, no. 4, pp. 2804–2821, 4th Quart., 2018.

[4] C. Yan, L. Fu, J. Zhang, and J. Wang, "A comprehensive survey on UAV communication channel modeling," *IEEE Access*, vol. 7, pp. 107769–107792, 2019.

[5] W. Khawaja, I. Guvenc, D. W. Matolak, U. Fiebig, and N. Schneckenburger, "A survey of air-to-ground propagation channel modeling for unmanned aerial vehicles," *IEEE Commun. Surveys Tuts.*, vol. 21, no. 3, pp. 2361–2391, 3rd Quart., 2019.

[6] M. Simunek, F. P. Fontán, and P. Pechac, "The UAV low elevation propagation channel in urban areas: Statistical analysis and time-series generator," *IEEE Trans. Antennas Propag.*, vol. 61, no. 7, pp. 3850–3858, Jul. 2013.

[7] M. Simunek, P. Pechac, and F. P. Fontan, "Excess loss model for low elevation links in urban areas for UAVs," *Radioengineering*, vol. 20, no. 3, pp. 561–568, 2011.

[8] L. Zeng, X. Cheng, C. Wang, and X. Yin, "A 3D geometry-based stochastic channel model for UAV-MIMO channels," in *Proc. IEEE Wireless Commun. Netw. Conf. (WCNC)*, 2017, pp. 1–5.

[9] D. Rieth, C. Heller, D. Blaschke, and G. Ascheid, "On the practicability of airborne MIMO communication," in *Proc. IEEE/AIAA 34th Digit. Avion. Syst. Conf. (DASC)*, 2015, pp. 1–10.

[10] A. Al-Hourani, S. Kandeepan, and A. Jamalipour, "Modeling air-to-ground path loss for low altitude platforms in urban environments," in *Proc. IEEE Global Commun. Conf.*, 2014, pp. 2898–2904.

[11] J. Holis and P. Pechac, "Elevation dependent shadowing model for mobile communications via high altitude platforms in built-up areas," *IEEE Trans. Antennas Propag.*, vol. 56, no. 4, pp. 1078–1084, Apr. 2008.

[12] D. W. Matolak, "Air-ground channels models: Comprehensive review and considerations for unmanned aircraft systems," in *Proc. IEEE Aerosp. Conf.*, Mar. 2012, pp. 1–17.

[13] Y. S. Meng and Y. H. Lee, "Study of shadowing effect by aircraft maneuvering for air-to-ground communication," *AEU Int. J. Electron. Commun.*, vol. 66, no. 1, pp. 7–11, 2012.

[14] R. Sun and D. W. Matolak, "Initial results for airframe shadowing in L- and C-band air-ground channels," in *Proc. Integr. Commun. Navig. Surveillance Conf. (ICNS)*, Apr. 2015, pp. 1–8.

[15] N. Schneckenburger *et al.*, "Modeling the air-ground multipath channel," in *Proc. 11th Eur. Conf. Antennas Propag. (EUCAP)*, Mar. 2017, pp. 1434–1438.

[16] X. Cai *et al.*, "Low altitude UAV propagation channel modelling," in *Proc. 11th Eur. Conf. Antennas Propag. (EUCAP)*, Mar. 2017, pp. 1443–1447.

[17] D. W. Matolak and R. Sun, "Air-ground channel measurements and modeling for UAS," in *Proc. IEEE Integr. Commun. Navig. Surveillance Conf. (ICNS)*, 2013, pp. 1–9.

[18] R. Sun and D. W. Matolak, "Over-harbor channel modeling with directional ground station antennas for the air-ground channel," in *Proc. IEEE Mil. Commun. Conf.*, 2014, pp. 382–387.

[19] D. W. Matolak and R. Sun, "Air-ground channel characterization for unmanned aircraft systems: The near-urban environment," in *Proc. IEEE Mil. Commun. Conf. (MILCOM)*, Oct. 2015, pp. 1656–1660.

[20] M. Rice and M. Jensen, "Multipath propagation for helicopter-to-ground MIMO links," in *Proc. MILCOM Mil. Commun. Conf.*, Nov. 2011, pp. 447–452.

[21] M. Simunek, F. P. Fontan, P. Pechac, and F. J. D. Otero, "Space diversity gain in urban area low elevation links for surveillance applications," *IEEE Trans. Antennas Propag.*, vol. 61, no. 12, pp. 6255–6260, Dec. 2013.

[22] T. J. Willink, C. C. Squires, G. W. K. Colman, and M. T. Muccio, "Measurement and characterization of low-altitude air-to-ground MIMO channels," *IEEE Trans. Veh. Technol.*, vol. 65, no. 4, pp. 2637–2648, Apr. 2016.

[23] K. Daniel, M. Putzke, B. Dusza, and C. Wietfeld, "Three dimensional channel characterization for low altitude aerial vehicles," in *Proc. 7th Int. Symp. Wireless Commun. Syst.*, Sep. 2010, pp. 756–760.

[24] D. Matolak and R. Sun, "AG channel measurements & modeling: Initial analysis & flight test planning," Dept. Comput. Sci., Ohio Univ., Athens, OH, USA, Rep. 2, 2012.

[25] W. G. Newhall *et al.*, "Wideband air-to-ground radio channel measurements using an antenna array at 2 Ghz for low-altitude operations," in *Proc. IEEE Mil. Commun. Conf. (MILCOM)*, vol. 2, 2003, pp. 1422–1427.

[26] E. Haas, "Aeronautical channel modeling," *IEEE Trans. Veh. Technol.*, vol. 51, no. 2, pp. 254–264, Mar. 2002.

[27] W. G. Newhall and J. H. Reed, "A geometric air-to-ground radio channel model," in *Proc. MILCOM*, vol. 1, Oct. 2002, pp. 632–636.

[28] M. Rice, R. Dye, and K. Welling, "Narrowband channel model for aeronautical telemetry," *IEEE Trans. Aerosp. Electron. Syst.*, vol. 36, no. 4, pp. 1371–1377, Oct. 2000.

[29] A. Dedryvere, B. Roturier, and B. Chateau, *A General Model for VHF Aeronautical Multipath Propagation Channel*, Aeronaut. Mobile Commun. Panel, Honolulu, HI, USA, 1999.

[30] P. Almers *et al.*, "Survey of channel and radio propagation models for wireless MIMO systems," *EURASIP J. Wireless Commun. Netw.*,

vol. 2007, no. 1, pp. 56–56, 2007. [Online]. Available: https://jwcn-eurasipjournals.springeropen.com/articles
[31] M. Wentz and M. Stojanovic, "A MIMO radio channel model for low-altitude air-to-ground communication systems," in *Proc. IEEE 82nd Veh. Technol. Conf. (VTC Fall)*, Sep. 2015, pp. 1–6.
[32] S. Blandino, F. Kaltenberger, and M. Feilen, "Wireless channel simulator testbed for airborne receivers," in *Proc. IEEE Globecom Workshops (GC Wkshps)*, Dec. 2015, pp. 1–6.
[33] H. A. Mendoza and G. Corral-Briones, "On the application of three dimensional hap MIMO model in UAV environment," *Veh. Commun.*, vol. 16, pp. 72–84, Apr. 2019. [Online]. Available: http://www.sciencedirect.com/science/article/pii/S2214209617302097
[34] E. T. Michailidis and A. G. Kanatas, "Three-dimensional HAP-MIMO channels: Modeling and analysis of space–time correlation," *IEEE Trans. Veh. Technol.*, vol. 59, no. 5, pp. 2232–2242, Jun. 2010.
[35] A. Abdi, J. A. Barger, and M. Kaveh, "A parametric model for the distribution of the angle of arrival and the associated correlation function and power spectrum at the mobile station," *IEEE Trans. Veh. Technol.*, vol. 51, no. 3, pp. 425–434, May 2002.
[36] S. S. Mahmoud, Z. M. Hussain, and P. O'Shea, "A geometrical-based microcell mobile radio channel model," *Wireless Netw.*, vol. 12, no. 5, pp. 653–664, 2006, doi: 10.1007/s11276-006-6061-0.
[37] M. Vazquez-Castro, F. Perez-Fontan, and S. R. Saunders, "Shadowing correlation assessment and modeling for satellite diversity in urban environments," *Int. J. Satellite Commun.*, vol. 20, no. 2, pp. 151–166, 2002, doi: 10.1002/sat.718.
[38] M. A. Vazquez-Castro, D. Belay-Zelek, and A. Curieses-Guerrero, "Availability of systems based on satellites with spatial diversity and HAPs," *Electron. Lett.*, vol. 38, no. 6, pp. 286–288, Mar. 2002.
[39] C. Tzaras, B. G. Evans, and S. R. Saunders, "Physical-statistical analysis of land mobile-satellite channel," *Electron. Lett.*, vol. 34, no. 13, pp. 1355–1357, Jun. 1998.
[40] S. Saunders and B. Evans, "Physical model of shadowing probability for land mobile satellite propagation," *Electron. Lett.*, vol. 32, no. 17, pp. 1548–1549, 1996.
[41] A. Bharti, R. Adeogun, and T. Pedersen, "Learning parameters of stochastic radio channel models from summaries," *IEEE Open J. Antennas Propag.*, vol. 1, pp. 175–188, 2020.
[42] R. Adeogun, "Calibration of stochastic radio propagation models using machine learning," *IEEE Antennas Wireless Propag. Lett.*, vol. 18, no. 12, pp. 2538–2542, Dec. 2019.

HORACIO A. MENDOZA received the Electronic Engineering degree from the National University of Misiones (UnaM), Misiones, Argentina, in 2004, and the Master of Science in Engineering degree from the National University of Cordoba, Argentina, in 2012. He is currently serving as a Professor and Researcher with the Digital Communication Laboratory (LCD), Universidad Nacional de Córdoba. Also is currently serving as a Researcher of the Grupo de Investigación y Desarrollo en Ingeniería Electrónica (GIDIE) with the Department of Electronic Engineering of the UNaM. His research interests lie in the fields of channel modeling and measurements and advanced digital modulation/reception techniques for MIMO Wireless Communication.

GRACIELA CORRAL-BRIONES received the Electrical and Electronic Engineering and Ph.D. degrees from the National University of Cordoba, Cordoba, Argentina, in 1991 and 2007, respectively. From 1991 to 1993, she was with the Center for Research in Materials, Cordoba, as a Research Fellow. From 1993 to 1996, she received a fellowship from CONICOR (Scientific and Technological Research Council of Cordoba) to develop analyzers for communication protocols. Since March 1996, she has been with the Digital Communications Research Laboratory, Department of Electronic Engineering, National University of Cordoba. Her research interests lie in the areas of wireless communications and signal processing, including multiuser detection, channel coding, and MIMO systems.